Universiteit Utrecht

Opleiding Natuur- en Sterrenkunde

Effects of local heating on resonances in photonic crystal nanocavities

Bachelor Thesis

Mark Mollema

Supervisors:

K.L. Perrier MSc

Dr. Sebastiaan Greveling

Prof. dr. A.P. Mosk

January 16, 2019

Abstract

Photonic crystals are materials that have a periodic dielectric function. These materials interact with light in a similar way that electrons do in a periodic electric potential. The properties of photonic crystals allow for a high degree of control of the propagation of light. Photonic crystals are promising in the development of a wide range of devices that exploit the control over the flow of light. We study an InGaP coupled resonator optical waveguide photonic crystal photonic crystal. The InGaP membrane contains optical cavities which show resonances at infrared frequencies. When the membrane is heated locally using a laser beam as a heat source we observe the redshifting of resonances and an increase of the FWHM of the resonance. The redshift of a resonance depends on where the heat is applied, which shows us information about the electric field profile and spatial position of a resonance. Furthermore, we observe blueshifting of resonances *after* the sample is heated.

Contents

1 Introduction

Advancements in semiconductor technologies have reshaped societies all around the globe. Our lives would be unimaginable without devices like computers or LEDs. This technological success has only been possible through our understanding of the underlying physics. For semiconductors, the theory is founded on electrons in periodic lattices spanned by ions[1]. The increasing demand for speed and efficiency motivates to find alternatives for semiconductor technologies. A likely candidate as a data carrier is light: through precise engineering of materials, light can exhibit similar behaviour as electrons in solids [2]. To design optical systems with similar functionality as their electrical counterpart photonic crystals can be used. These crystals have a periodic dielectric function with which photons interact in a similar way as electrons do in an ion lattice.

Photonic crystals allow for the control of the propagation of light, for example a waveguide restricts the flow of light to only a certain direction. An other feature of photonic crystals is that they can have intentional defects in their crystal structure which allow for the confinement of the electric field at certain frequencies[3]. These local defects are called (nano)cavities and allow for resonances of electromagnetic waves. For the future application of photonic crystals it is import to understand the behaviour of such materials under the influence of temperature. In this thesis we study the effect of local heating on resonances in photonic crystal nanocavities.

In this thesis we want to address the question: 'What is the effect of optical local heating on resonances in photonic crystal nanocavities?' Our results show that the resonances shift in wavelength when the sample is locally heated. The mode profile can be determined from the redshift as a function of where the heat is applied. Furthermore, we observe that the quality factor of a resonance decreases when the heat is applied; the Q factor and redshift behave differently depending on pump position. We also observe a slow blueshifting of resonances after the cavities are illuminated by blue light. The time scale of this effect is on the order of minutes which is much longer than the heating and cooling down of the sample, which is on the order of microseconds [4]. Possible origins are the evaporation of a thin film of water on the sample[5] or the slight ionization of the sample surface [6].

For the precise positioning of the laser-induced local heating, we use a fast steering mirror (FSM). This is a mirror that can rotate around two axes with high precision. In this thesis we also develop a method for calibrating this apparatus, so that we can move the position of the heat source with a precision of about 100 nm.

2 Experimental setup

The sample that we use in this thesis is a InGaP photonic crystal membrane. The membrane contains a triangular lattice of air holes which form the regions with a low dielectric constant. A row of these holes is omitted forming a waveguide. The surrounding crystal lattice prohibits any light travelling into the crystal; the light can only travel along the waveguide direction. Using a lensed fiber we inject infrared light into the waveguide. Parallel to the input waveguide there the barrier waveguide; this waveguide contains the resonant cavities. The resonant cavities are formed by shifting some of the air holes from their lattice positions. This creates a local defect in which resonances can occur.

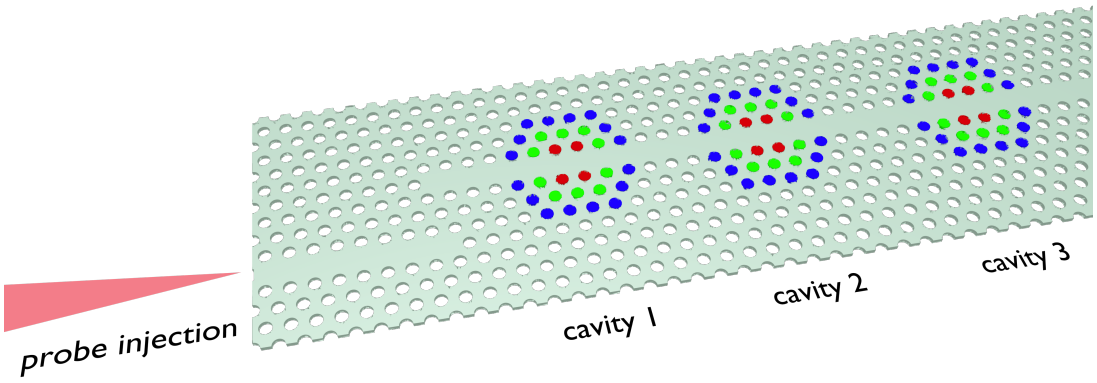

Figure 1: Sketch of the sample. The thickness of the membrane is 180 nm and the lattice constant is 485 nm. The coloured holes indicate the holes that have been shifted from their lattice positions to create the cavities. IR light can couple from the input waveguide into the cavities via evanescent coupling.

A fraction of light scatters from the photonic crystal membrane. For applications of photonic nanocavities this might be disadvantageous however it does allow us the measure resonances in a simple way. We assume that the out-of-plane scattering (OOPS) in the cavity is proportional to intensity of the light in the cavity. We detect the scattered light using a photodiode, the signal of which is amplified with a factor 10^8 using a Femto amplifier.

We image the sample with two different cameras; one that is sensitive to IR light and one that is sensitive to blue light. The blue camera is used for imaging the pump spot, which is crucial for the FSM calibration. The IR camera is used to make an easy identification of resonances and for aligning the lensed fiber.

The source of IR probe light is a Santec TSL-710 tunable laser. This laser allows us to measure the OOPS for different wavelengths in rapid succession. We are able to scan 1 nm/s with a resolution of a picometre. Before the light gets to the sample it goes through a large array of fibers and other devices to control and monitor the IR light. We alter the IR probe power using an electro-optic modulator which we control using a function generator which, for our goals, outputs a constant DC voltage.

The source of the heat is a 405 nm OBIS continuous-wave diode laser. The light is focussed on the sample using a 0.4 NA objective.

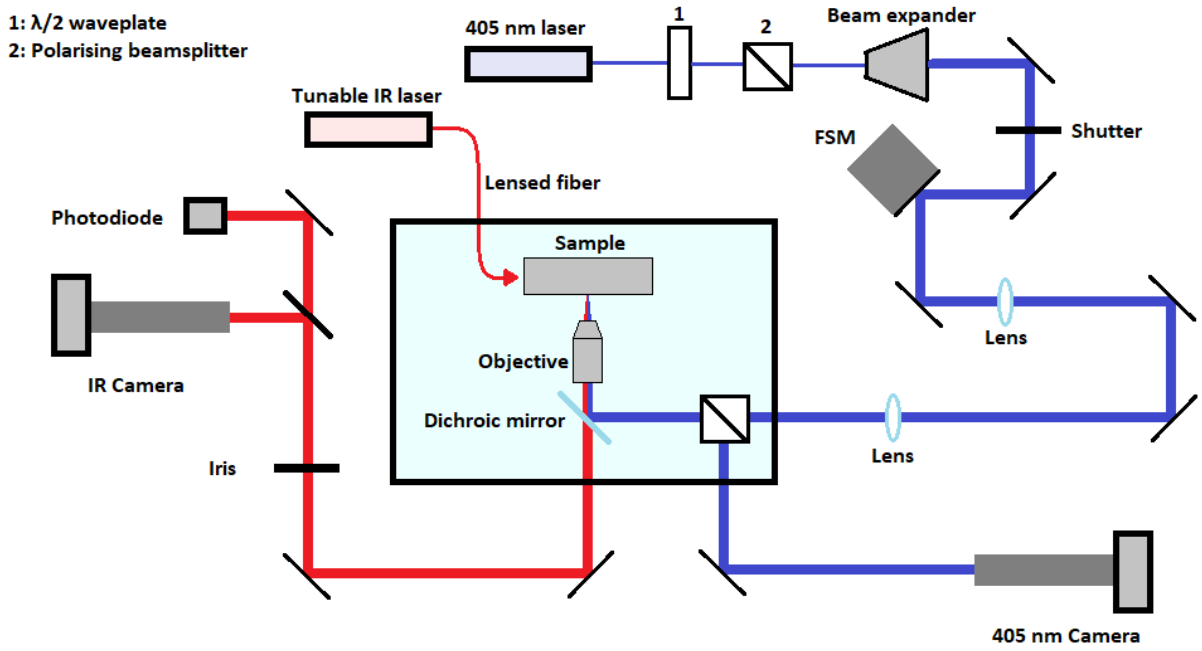

Figure 2: Schematic of the relevant parts of the setup. The red and blue lines depict the paths of the infrared and blue light respectively. IR light is focussed from the polarisation maintaining lensed fiber into the input waveguide. The mirror in front of the IR camera can be folded down to switch between the camera and photodiode. The combination of the rotatable $\lambda/2$ waveplate and the polarising beamsplitter allows for attenuating the blue laser beam. The iris allows for controlling from which part of the sample IR light is collected.

We control the movement of the blue pump beam using a fast steering mirror (FSM) which is a mirror that can rotate around two axes allowing for the horizontal and vertical movement of the pump spot on the sample. The two lenses in figure 2 form a telescope. The way the FSM is placed is that the blue beam strikes the mirror surface in the focus of the first lens of this telescope. This means that a change of angle of the FSM leads to only movement of the beam on the objective, i.e. the angle with which it strikes the objective is not changed. The beam expander is positioned such that the beam is collimated on the FSM.

3 Theory

In this section we will briefly describe some theoretical results which are necessary to understand the results we will present in this thesis. Heating the photonic crystal perturbs the dielectric constant locally. This change in dielectric constant shifts the resonance. Using first order perturbation theory the correction to the resonance wavelength can be calculated [7].

$$\Delta\lambda = \frac{\lambda}{2}\frac{\int \Delta\epsilon(\mathbf{r})|\mathbf{E}(\mathbf{r})|^2 d\mathbf{r}}{\int \epsilon(\mathbf{r})|\mathbf{E}(\mathbf{r})|^2 d\mathbf{r}} \tag{1}$$

Where λ is the wavelength, $\epsilon(\mathbf{r})$ the dielectric constant and $|\mathbf{E}(\mathbf{r})|^2$ is the norm of the electric field which we will call the mode profile. Assuming that the change in dielectric constant is linearly proportional to the local temperature and noting that the terms in the denominator are just a constant as is the term in front, this can be rewritten as:

$$\Delta\lambda = \alpha \int \Delta T(\mathbf{r} - \mathbf{r}_0)|\mathbf{E}(\mathbf{r})|^2 d\mathbf{r} \tag{2}$$

Where α is some proportionality constant and $\Delta T(\mathbf{r} - \mathbf{r}_0)$ is the temperature perturbation centred around the pump position $\mathbf{r}_0$. Mathematically speaking, this means that the redshift is proportional to the convolution of the thermal and electrical mode profiles. Using a deconvolution one could recover the mode profile[8], for this the thermal profile first needs to be calculated. The above equation can be interpreted as follows: the redshift is given by the overlap between the electrical field in the cavity and the thermal profile caused by the pump light. When this overlap is large, the redshift is also large.

4 Calibration of the fast steering mirror

In order to demonstrate the effects of local heating on the resonances of photonic crystal nanocavities the source of heat, i.e. the blue laser beam, has to be positioned accurately. To achieve this goal we use a fast steering mirror which allows for the automation of measurements and sub-micrometre precision of the position the pump beam. A fast steering mirror (FSM) is a type of mirror which can pivot about two axes and for this reason can create both horizontal and vertical movement of the pump beam on the sample. It uses four voice coil actuators (like in a loudspeaker) to pivot the mirror. Because the mirror is only kept in place by these actuators it is quite sensitive to vibrations. To counteract this behaviour, the FSM uses an internal feedback loop to correct for these unwanted motions to keep the chosen angle at the desired position.[9]

The FSM is controlled by applying voltages (called V_x and V_y) to both of the voltage inputs on the controller of the FSM, which then moves the mirror to the desired angles. This movement is generally quite fast and the position of the beam on the sample is stable after much less than a second. If the step is much less than 0.05 V, the process of stabilisation is not visible on the camera by eye. However, if larger steps are taken, for example 1 V, it becomes clearly visible than the mirror slightly overshoots the desired position and then moves to the right position. Still, this takes less than a second.

The goal of the calibration is to convert the desired position of the pump beam to voltages which can be applied to the input of the FSM. Therefore we propose a simple model for how the beam position depends on the applied voltage, which will be explained in the next section.

4.1 Model for the calibration

To convert beam positions into voltages which can be applied to the input of the FSM controller, some assumptions need to be made. In general, the beam position depends on the voltages via a function which could be calculated using a ray transfer matrix method for Gaussian beams[10]:

$$\begin{pmatrix} p_x \\ p_y \end{pmatrix} = \begin{pmatrix} f(V_x, V_y) \\ g(V_x, V_y) \end{pmatrix} \tag{3}$$

Where p_x and p_y are the coordinates of the beam and $f(V_x, V_y)$ and $g(V_x, V_y)$ are the functions which convert the voltages to the positions, but also depend on the optics and their positions in the beam path. To make the calibration more straightforward, we linearise this expression. This linearisation is expected to be accurate because the range of voltages (and thus FSM angles) will be quite small for the planned application, the range of movement of the beam spot will be about 40 µm for the measurements in section 5. The accuracy of the assumption of linearity will also be tested in section 4.3. This assumption of linearity implies:

$$\begin{pmatrix} p_x \\ p_y \end{pmatrix} \simeq \begin{pmatrix} \nabla_{\vec{V}}\, f|_{\vec{V}=\vec{V}_0} \cdot \left(\vec{V} - \vec{V}_0\right) \\ \nabla_{\vec{V}}\, g|_{\vec{V}=\vec{V}_0} \cdot \left(\vec{V} - \vec{V}_0\right) \end{pmatrix} + \begin{pmatrix} f(V_{0,x}, V_{0,y}) \\ g(V_{0,x}, V_{0,y}) \end{pmatrix} \tag{4}$$

Where $\nabla_{\vec{V}}$ is a vector operator differentiating to V_x and V_y, and $\vec{V_0}$ is the voltage at which the linearisation occurs. The above equation is a two variable first order Taylor expansion around $\vec{V_0}$. This can be much simplified by realising that all the terms involving f and g are just numbers and the final term on the right is the beam position at $\vec{V} = \vec{V_0}$, which we will call $\vec{p_0}$. This yields:

$$\vec{p} = \mathbf{A}\big(\vec{V} - \vec{V_0}\big) + \vec{p_0} \tag{5a}$$

$$\mathbf{A} = \begin{pmatrix} \alpha & \beta \\ \gamma & \delta \end{pmatrix} \tag{5b}$$

Where the matrix $\mathbf{A}$ with coefficients which are yet to be determined (which is exactly the goal of the calibration). This expression can be inverted to find the voltages for a certain beam position:

$$\vec{V} = \mathbf{A}^{-1}\big(\vec{p} - \vec{p_0}\big) + \vec{V_0} \tag{6}$$

4.2 Determining the calibration matrix

The coefficients as mentioned in equation 5a have to be determined in order to be able to use equation 6. The exact values of these coefficients will be determined by fitting p_x and p_y to both V_x and V_y. The way this works becomes obvious when equation 5a is written out, we will only do this for p_x; the method for p_y is identical.

$$p_x = \alpha(V_x - V_{0,x}) + \beta(V_y - V_{y,0}) + p_{0,x} \tag{7}$$

The slope of the fit of p_x to V_x and V_y is given by α and β respectively. The way this will be done is as follows: the beam is first positioned to a certain position $\vec{p_0}$, which ideally should be the position around which measurements with the pump spot will be done. This position $\vec{p_0}$ has a corresponding voltage $\vec{V_0}$. Around this voltage $\vec{V_0}$, two lines are drawn. One line has V_x constant, the other has V_y constant. The intersection of the two lines is $\vec{V_0}$. The length of these lines should be such that the difference in voltage between the ends of the line corresponds to a change in position of the beam which is roughly equal to the size of the part of the sample with the cavities. This range also happens to be the range in which non-linearities are negligible. This range is illustrated in appendix A. On the two lines a number of equidistant voltages are chosen for which the beam positions are determined. By fitting the beam positions to the voltages, the calibration matrix is determined as described earlier.

4.2.1 Measuring the beam position

For carrying out the calibration, it is necessary to determine the beam positions with high precision. This goal is achieved by making images using the camera which is only sensitive to blue light. When the blue laser illuminates the sample, a group of pixels light up. We define the beam position as the weighted average of the pixels:

$$\vec{p} = \frac{\sum_i I(\vec{p_i})\vec{p_i}}{\sum_i I(\vec{p_i})} \tag{8}$$

Where $\vec{p}$ is the position of the pump beam on the camera measured in pixels, the sum runs over all pixels $\vec{p}_i$ and $I(\vec{p}_i)$ is the pixel readout of the camera (basically the intensity). This is very similar to the centre of mass. It is of great importance that the camera is not overexposed; otherwise pixels have a readout which is not proportional to the intensity and equation 8 no longer holds. The way this equation is employed in practice is slightly different: there is always some noise present in the image and there are interference fringes around the beam spot. For these reasons, we only sum over the pixels above a certain threshold; it was found empirically that a threshold value of ten percent of the maximum intensity of the beam spot worked best.

4.2.2 Results of the calibration

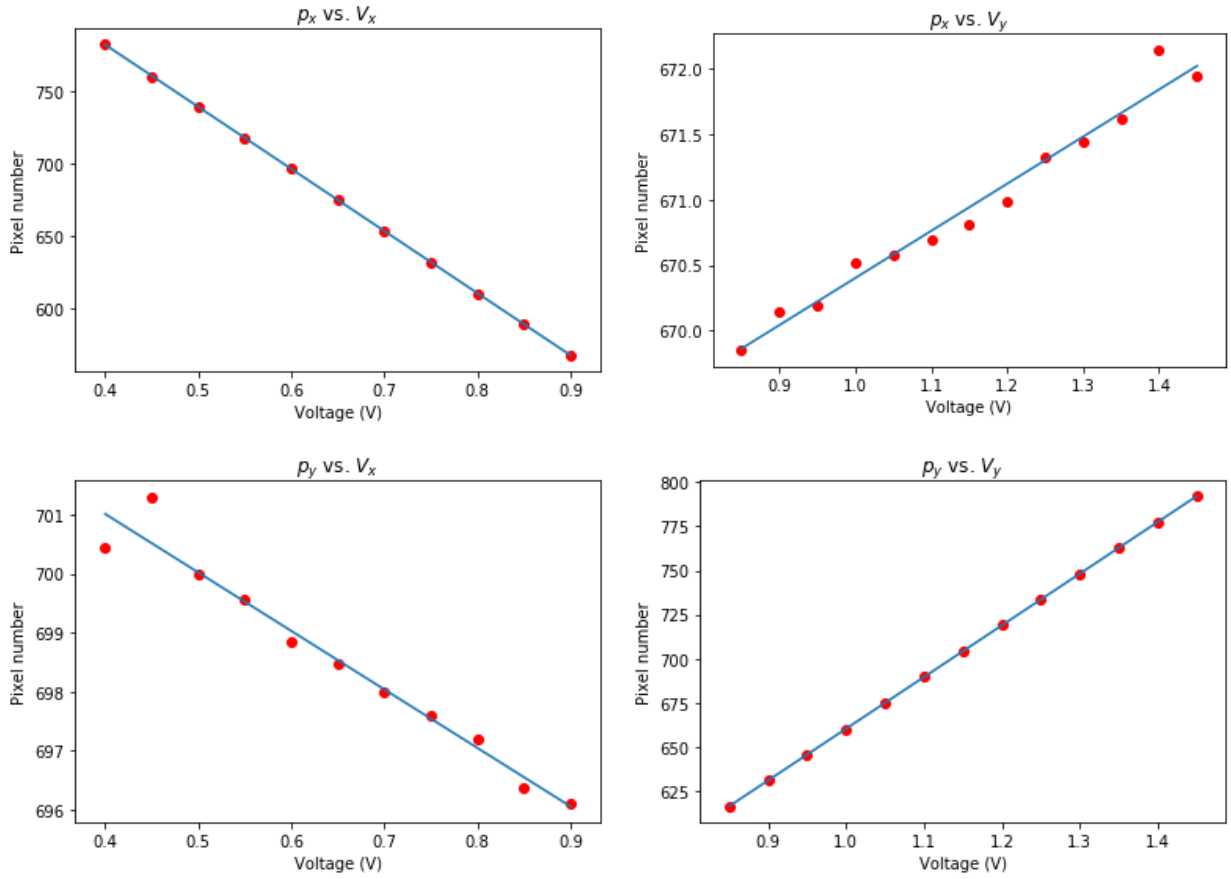

Figure 3: The fits as described in the beginning of section 4.2. The above graphs show that the response of the beam positions p_x and p_y are strong to changes in V_x and V_y respectively. Whereas responses are weak for p_x and p_y are weak when V_y and V_x respectively are changed. This can be attributed to the positioning of the FSM and camera; a change in V_x and V_y should lead to horizontal and vertical movement of the pump spot respectively.

Because the responses of p_x and p_y are weak when V_y and V_x respectively are changed, the corresponding fits show the shaking of the beam spot, even if the voltage is kept constant.

This can be seen by the large relative deviation of the data from fitted function. This effect will be quantified in section 4.4.

The units that are used for the position of the beam spot are pixels on the camera. The reason this is done is that these units are easier to work with: for measurements which are described in section 5, the scanning range is determined by looking on the camera, which uses pixels as units. Furthermore, they can always be converted to more conventional units of length like micrometres using known lengths of the sample.

The matrix as described by equation 5b is given by the slopes in figure 3. This looks as follows:

$$\mathbf{A} = \begin{pmatrix} \alpha & \beta \\ \gamma & \delta \end{pmatrix} = \begin{pmatrix} -427.3 \pm 0.4 & -9.9 \pm 0.6 \\ 3.6 \pm 0.2 & 292.1 \pm 0.2 \end{pmatrix} \tag{9}$$

The units of these values are pixels per Volt.

4.3 Effects of non-linear beam response

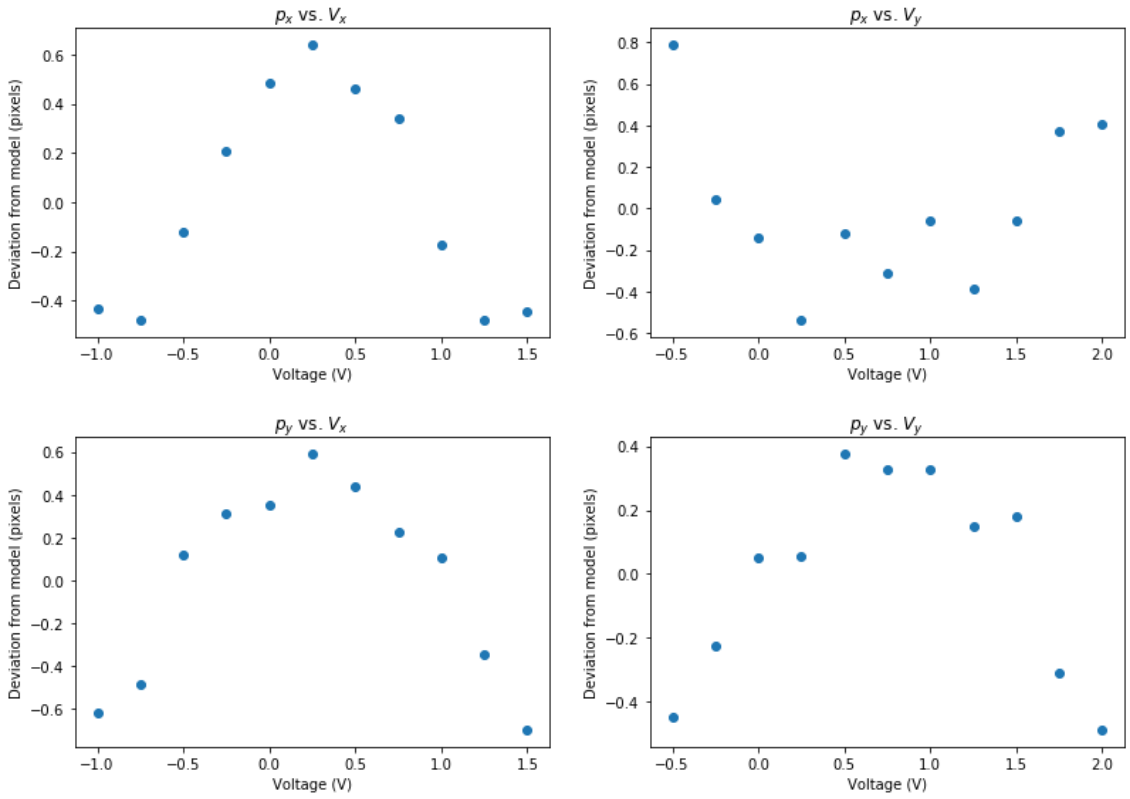

Figure 4: Fit residuals for the calibration procedure if the entire camera is used. Note the approximately parabolic shape of the residuals.

In order to study to what degree the assumptions made to derive equation 5 are valid, the calibration is carried out using the full range of the camera. Here we plot only the deviation of

the beam spot from the fitted function, i.e. the fit residuals. The actual fits are in appendix B.

Figure 4 shows that the assumption of linearity breaks down if the entire range of pixels of the camera is used for the calibration. This can be seen by the fact that the fit residuals are are a curved shape, which means that the linear function that has been fitted to the data is not a very good model.

Figure 4 shows that the assumption of linearity is sufficient for our goals. Within the range of about 0.5 V, which is the range that will be used for actual measurements, the error of the beam position caused by non-linearities is much less than a pixel.

If for some reason a higher degree of precision over a wider range of voltages is required, and therefore the influence of non-linear behaviour becomes important, a different method of calibration needs to be used. We propose two different methods: firstly, you could expand equation 5 up to a higher order. However, this leads to cross-terms of V_x and V_y and therefore our simple method of using a 'cross' of voltages no longer works. Secondly, you could use an actual physics based fitting function, based on the items used in the experimental setup, e.g. lenses. However such a function does not account for any possible present non-linearities inherent to the FSM, also the inversion as done in equation 6 would be much more cumbersome.

4.4 Measurement of beam jitter

When the FSM is put at a constant voltage, one would expect that the beam spot is stationary. However, this is not the case. It is visible by eye that the beam spot shakes around a certain position, which we will call jitter. This is quantified by measuring the beam repeatedly at the same voltage. The measurement has been automated by using a Python script which makes images of the sample while it is hit by the pump beam. This is done for 2000 different images. Over a course of five minutes 2000 images were made, which means that about 7 images were made per second. For each of these images the beam spot was determined as defined by equation 8.

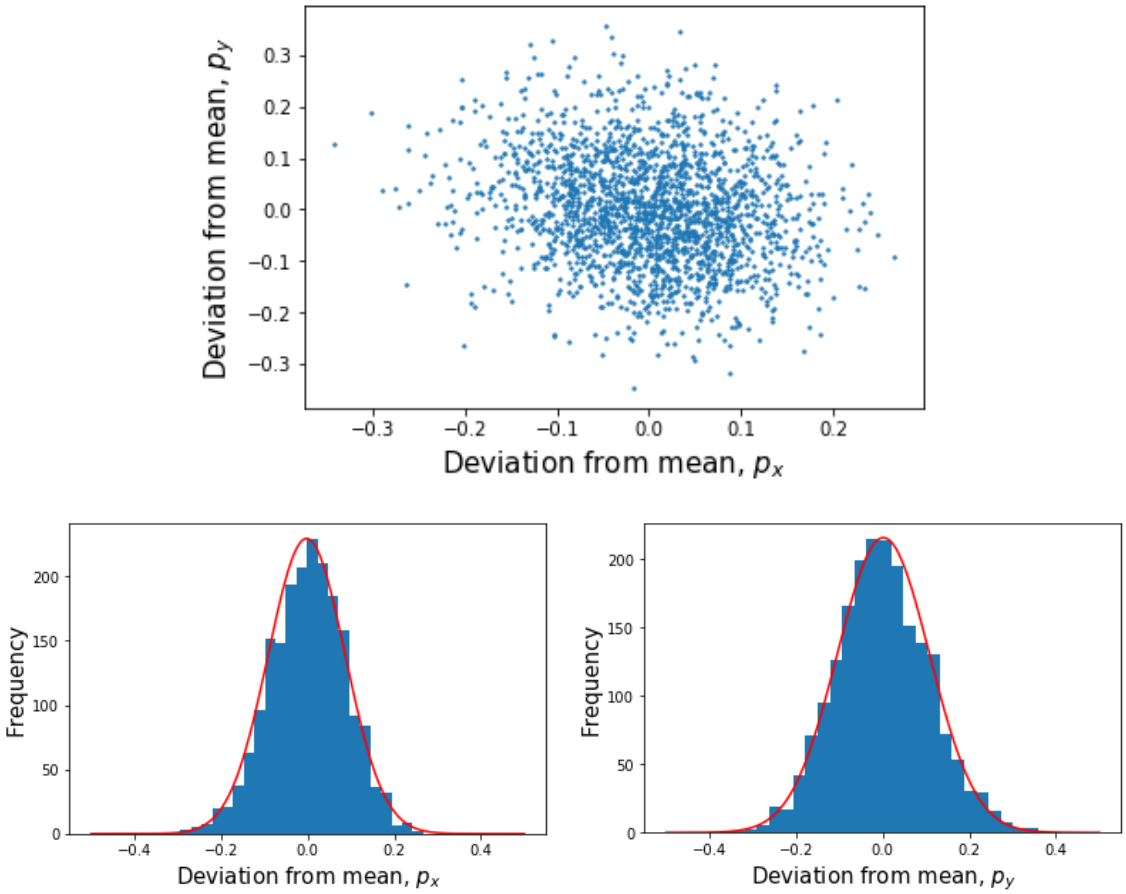

Figure 5: Results of the jitter measurement. The top plot shows the results of the beam positions for all the images. This shows that the jitter is symmetric around the mean in all directions. The bottom two plots are histograms that show the distribution of beam positions around the mean for both p_x and p_y. The red curves are both Gaussians that have been fitted to the histograms which show a reasonable agreement.

The standard deviation of the position in the direction of p_x, σ_x, is 0.09 pixel. The standard deviation for p_y, σ_y is slightly larger: 0.11 pixel. These uncertainties are built up of the size of the actual jitter, but also the error that has been introduced by our method of determining the beam position.

We have not yet discussed the origins of the jitter. There are three likely causes. The most likely cause is that the shaking is caused by air currents directly on the FSM. This theory is supported by the fact that the beam jitter greatly diminished after the FSM was enclosed in a box. For this reason the air around the FSM was much more stationary, because air currents arising from surrounding equipment could no longer reach the FSM. A second possible cause is that the mirror moves due to vibrations present in the optical table. The reason the FSM is so sensitive is that the mirror is only suspended by voice coil actuators which have a low spring constant. [9]. A final cause could be that the shaking of the mirror is caused by the active stabilisation that the FSM controller unit carries out, but this could also just counteract the previous two causes.

What has not been determined by these measurements is the time scale at which the jitter occurs. This can be significant for the following reason: if the time scale is very short, i.e. the jitter is very fast, the effect on the thermal profile would be that the profile gets slightly wider than one would expect on the size of the beam spot alone. This means that the heat diffusion 'smooths out' the jitter. Whereas if the jitter is slow, i.e. much slower than the typical time scale of the heat diffusion, the corresponding thermal profile will also shake, along with the pump beam. This might be of importance for highly precise measurements. To measure this time scale, simply making images with a large interval is insufficient. One would have to use a camera with an adequate frame rate to make a short film of the beam spot while it shakes to determine the typical time scale.

Jitter is a slight movement of the beam spot around the equilibrium position, but this position also moves. This movement happens on a much longer time scale; days instead of less than a second. The way this manifests is that the beam position $\vec{p}$ is no longer at $\vec{p}_0$ when $\vec{V} = \vec{V}_0$. This can be interpreted as that $\vec{p}_0$ moves around in time. The range of motion is about a micrometre, so a couple of pixels (it has not been measured exactly). Fortunately this does not mean the entire calibration needs to be carried out all over; simply replacing the value of $\vec{p}_0$ with the new beam position at $\vec{V} = \vec{V}_0$ is sufficient. The most likely cause of this type of movement is changes in temperature and/or humidity which result in slight movement of all the mirrors that are needed to get the blue laser beam to the sample.

4.5 Test of the calibration

To test the calibration, we have done a procedure which is similar to the measurements that will be discussed in a later section. Using equation 6 and the matrix in equation 9, the voltages have been calculated that move the beam horizontally across the camera in 30 steps.

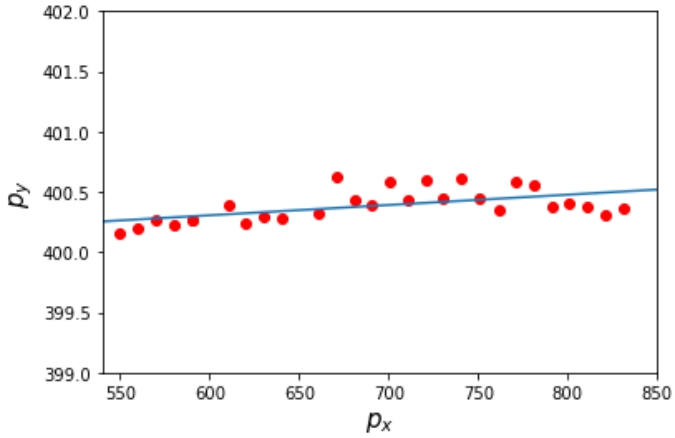

Figure 6: Results from the test of the calibration. Voltages were calculated such that beam spot moved from $p_x = 550$ to $p_x = 830$ with p_y constant at 400, in 30 steps. Three points fall outside this plot due to errors that were made when the voltages were applied manually. The blue line is a fit to the points and indicates a minor trend upwards.

Figure 6 shows that using our method of calibration, we are able to move the beam spot horizontally with great accuracy. The blue line shows a fit to the points; it only moves upward about 0.2 pixel over the range of 300 pixels. The standard deviation of the beam position in the direction of p_y is 0.13 pixel, which is only slightly larger than the values determined by the jitter measurement of 0.10 pixel. This larger standard deviation also indicates that the beam does not truly move horizontally. However, this accuracy is sufficient for the measurements that will be done in the rest of this thesis.

5 Effects of local heating on resonances

In this section we will discuss the measurements that were carried out using the calibration from the previous section. We will study the behaviour of different resonances under the effect of local heating caused by the light of the blue pump laser. All measurements involve scanning of the sample using the blue pump laser, while simultaneously measuring the cavity response using the out-of-plane scattering (OOPS). Most importantly, we will look at how resonances shift in wavelength (redshift) depending on the position of the heat source.

5.1 Setting up a measurement

Before measurements can be done some preparations need to be made, which we will describe here. The first step is the alignment of the input fiber from where the IR light gets to the waveguide. This is done by parking the laser at a known resonance wavelength such that a significant amount of light gets scattered from the cavities. Using the IR camera we can look at the intensity of the light that gets scattered. Moving the fiber using piezos varies the intensity of the scattered light; the position that maximises the intensity is the proper position of the fiber.

After the fiber is aligned, we move the objective horizontally such that the iris closes on the point halfway on the barrier waveguide. Then we open the iris again so that we can see as much as possible but *not* the input waveguide, which causes a lot of background scattering.

Then on the blue camera the focus and $\vec{p}_0$ of the beam spot will be checked. The beam is focussed by the objective; moving it in the direction perpendicular to the sample alters the focus. We position the objective in such a way that the beam spot is focussed in an area that is as small and symmetric as possible. This is done by eye using the camera. Then we remeasure $\vec{p}_0$ by applying $\vec{V}_0$ to the FSM and determining the beam position several times (about 10x) as described by equation 8, the average of which will be the new position $\vec{p}_0$.

Finally we need to determine the required power of the IR laser. Since we want to study the effects of external heating, we want to keep the heating caused by the IR light to a minimum. Secondly, the IR power need not be too low, otherwise the intensity of the OOPS is too low to actually detect anything. Both goals are achieved by repeatedly making OOPS spectra of the resonance that we want to measure, while simultaneously altering the IR power by changing the DC voltage of the function generator that is applied to the modulator. When the line shape of the OOPS spectrum is a symmetric Lorentzian we can conclude that the influence of heating from the IR light is negligible and therefore we have found the appropriate power.

5.2 Experimental procedure

The procedure of acquiring data has been standardised and automated for reproducibility and precision. Firstly, the positions that are to be scanned are determined by looking at the camera. From these positions the corresponding FSM voltages are calculated using the calibration and equation 6. We start each measurement with a reference scan, which is

making an OOPS spectrum without the pump beam. We scan over a range of wavelengths such that this range captures the entire Lorentzian line shape of the resonance, while also offering enough room that even the redshifted resonance is fully captured. We let the IR laser scan from short to long wavelengths (forwards) and also backwards; the signal that we use is the average of these two. For a single resonance, one nanometre is a sufficient scanning range since the resonances we study are quite sharp. After the reference scan the FSM is put to the first entry in the list of voltages for which will we measure the cavity response. The shutter is opened and immediately we measure the OOPS in the same way as before. Then the shutter is closed, we wait 1 second to let the sample cool down and we do another reference scan. This procedure is repeated for all the different beam positions, which means that each spectrum with the pump beam has a corresponding reference spectrum.

5.3 Spectrum analysis

For each measurement of the cavity response, we are mostly interested in the wavelength and linewidth of the resonance. This is determined by fitting a Lorentzian function to the OOPS data of the average of the forwards and backwards scan of the IR laser. This function has the following form [11]:

$$I(\lambda) = \frac{I_0}{1 + \left(\frac{\lambda - \lambda_0}{\gamma}\right)^2} + C \tag{10}$$

Where λ is the wavelength, λ_0 is the wavelength of the resonance where the OOPS signal is the strongest, γ is the linewidth (2γ is the full width at half maximum), I_0 is the maximal intensity of the resonance in the OOPS signal, and C is some constant to account for the noise.

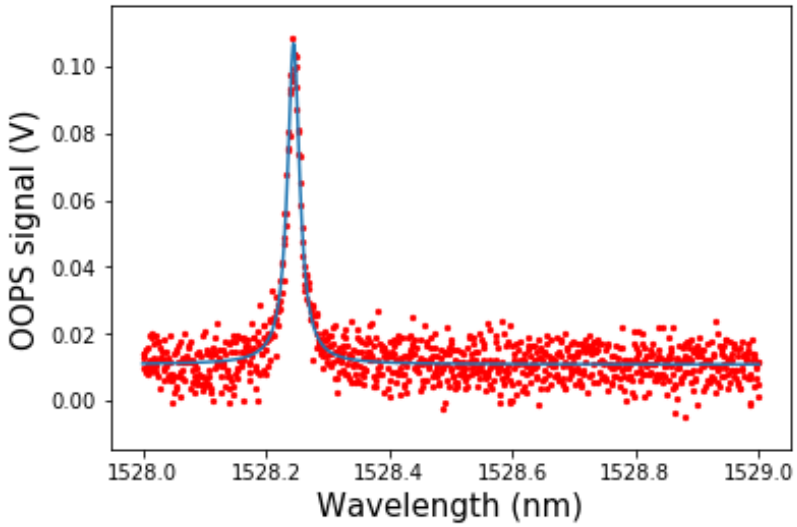

Figure 7: Example of a fit to the OOPS signal. The red dots indicate the OOPS signal for each wavelength, the blue line is a fit to this data. For this spectrum the resonance is at $\lambda = 1528.2453$ nm.

Figure 7 shows that we can measure resonance wavelengths with a precision of up to a

picometre. It is of great importance that the initial guess for the fit parameters is good. For the measurements with the scanning of the pump spot, the first initial guesses are found manually. For each following spectrum, the fit parameters of either the most recent reference spectrum or spectrum with pump beam are used. This assures that the initial guess is never too far off and that the fitting procedure converges to the right values.

5.4 One dimensional pump scan

Here we present the results of effects of local heating on two different resonances. These resonances were chosen for the reason that they showed a strong signal in OOPS and were isolated, i.e. there were no other resonances with a similar wavelength. The unpumped cavity response for both resonances are in appendix C. For these measurements we have scanned the blue pump spot over the barrier waveguide starting about 10 micron left of the barrier waveguide and ending 10 micron to the right in 175 steps, yielding a step size of about 200 nm. The FWHM of the pump spot is 0.8 µm, this has been determined by fitting a Gaussian to an image of the beam spot. The measurements were also repeated, but instead scanning from right to left. We look at the resonance redshift caused by the blue pump beam: these are determined by subtracting the most recent reference resonance wavelength from the resonance wavelength with the pump laser.

5.4.1 Resonance at $\lambda = 1530.8$ nm

All the results presented in this section (5.4.1) originate from the same dataset.

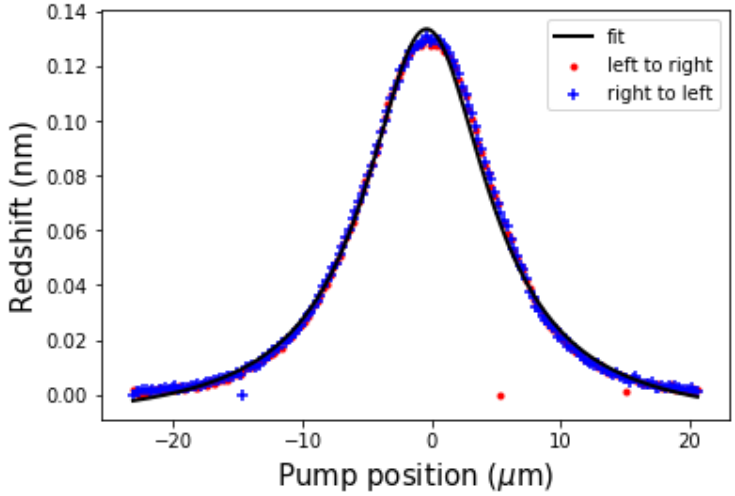

Figure 8: Redshift of resonance for different pump positions. There are 3 individual measurements which show a redshift of approximately zero; this is due to a malfunctioning of the shutter which would not open and therefore the blue beam could not heat the sample. The units on the x-axis are chosen in a way such that the origin is halfway the waveguide with the cavities.

Figure 8 shows that our measurements are repeatable and can be described by a Lorentzian

function, which implies that the mode profile can also be described by a Lorentzian, because of the result of first order perturbation theory (equation 2) and the fact that the temperature profile is also Lorentzian and that the convolution of two Lorenztians yields another Lorentzian.

The FWHM of the redshift profile is 11.6 ± 0.2 µm, which is roughly double of that what one would expect based on similar measurements [4]. This discrepancy could be caused by two factors: either the mode profile is much wider or the beam is not scanned directly over the wave guide but instead there is a slight offset to the top or bottom, which would give a wider temperature profile on the wave guide.

Figure 8 could be used to find out the spatial position of the resonance. In this case, the resonance is located at x = -0.38 µm, which is given by the centre of the Lorentzian function; this is where is overlap between the mode profile and the temperature profile is the largest. The profile in figure 8 is determined by comparing the resonances with pump beam to reference spectra without pump beam. The need for repeatedly making reference spectra becomes obvious when all the reference resonance values are plotted:

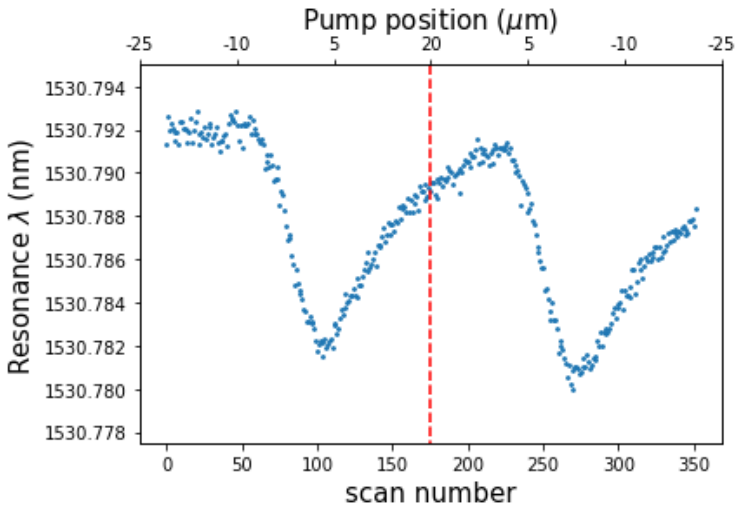

Figure 9: Plot of all the reference resonance wavelength in sequence. These values are for the entire measurement, so the back-and-forth movement of the pump beam, meaning that at the vertical line the movement of the beam reverses.

Figure 9 shows that the resonance wavelength for the unpumped cavities is not constant. The moment the beam spot comes close to the cavity, at about scan 60, the resonance starts to blueshift. This effect is cumulative; all the while the beam spot is close to the cavity, the resonance blueshifts further. Once the pump spot is sufficiently far removed, the resonance wavelength decays back to its original value. On the return movement of the beam spot a similar shift happens. The time in between individual reference scans is about 10 seconds; based on this we can estimate the decay time for the blueshift; this is on the order of several minutes.

The origin of the blueshifting is unclear: it might be tied to water film evaporation on the sample, as has been suggested before [5]. If this is the case, blueshifting is tied to the thermal profile. However the blueshifting starts at a later beam position and ends earlier than the redshifting, indicating that it might be related to the *beam* profile. The blue light might be able to catalyse a certain reaction or it is possible that the sample gets slightly ionised though the two-photon photoelectric effect [6].

The heating does not just shift resonances; the width of the resonance spectrum also changes. In figure 10 we plot the full width at half maximum as a function of the pump position. The FWHM dependence on the heating shows roughly similar behaviour as that of the redshift profile. However, The FWHM profile shows two peaks, the origin of which is unknown.

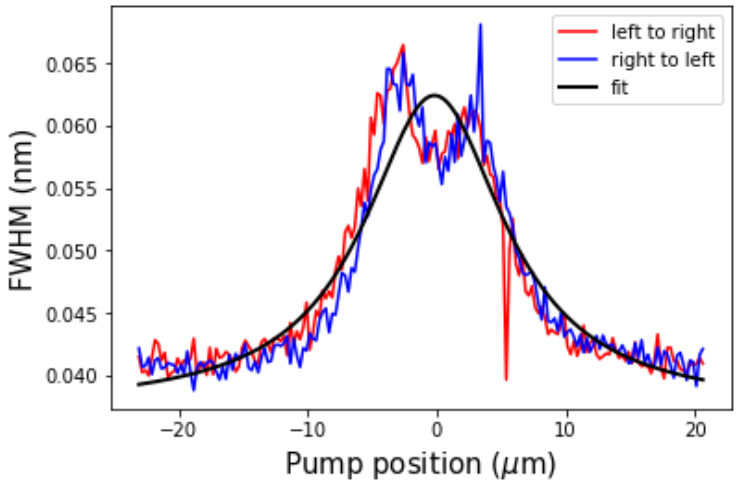

Figure 10: FWHM as a function of pump position. The red line shows an anomaly at $x = 5$ µm, this is due to the same shutter malfunction as mentioned earlier. The fits for the peaks of the FWHM for both scans are presented in appendix D. The black line indicates a Lorentzian fit to the blue line, the FWHM of which is 13.2 ± 0.7 µm which is not a very significant difference from the FWHM of the redshift profile.

Finally, in figure 11 we observe a reduction in the OOPS intensity the more redshifted the resonance is. A likely cause is that the resonance is tuned farther away from the photonic cavity band and therefore reducing the coupling to the input waveguide [4].

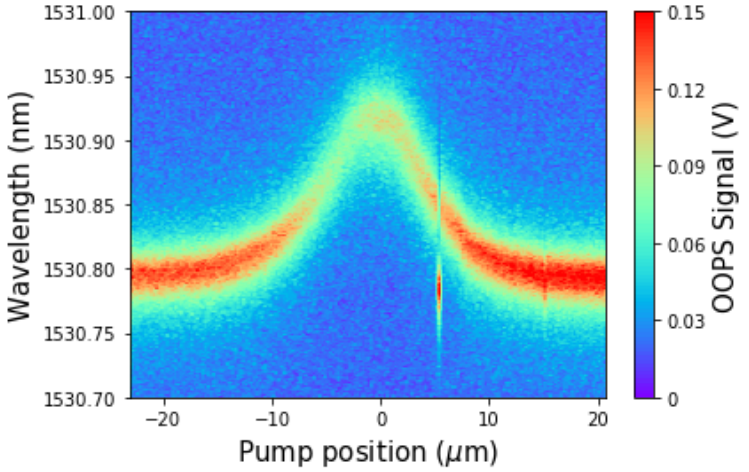

Figure 11: λ as a function of and pump position and OOPS signal for the left to right scan. The horizontal line at $x = 5$ µm is caused by the shutter malfunction. Note that although the shape of the curve is similar to the one in figure 8, it is not identical since it does not account for the blueshift of the reference resonances.

5.4.2 Resonance at $\lambda = 1528.2$ nm

All the results presented in this section (5.4.2) originate from the same dataset.

We have repeated the same measurements as in the previous section; however this time for a resonance at a different wavelength. Based on the OOPS spectrum one would not expect that these resonances are different: they both have a Lorentzian line shape. However the resonances differ significantly when the sample is heated locally.

The redshift profile in figure 12 is much wider than in figure 8 and this profile shows a plateau; a region in which the redshift roughly stays constant. The width of this plateau is about 12 µm. The plateauing of the redshift profile indicates that the mode profile is relatively constant over a certain range, based on equation 2. This implies the electric field is delocalised along the waveguide direction.

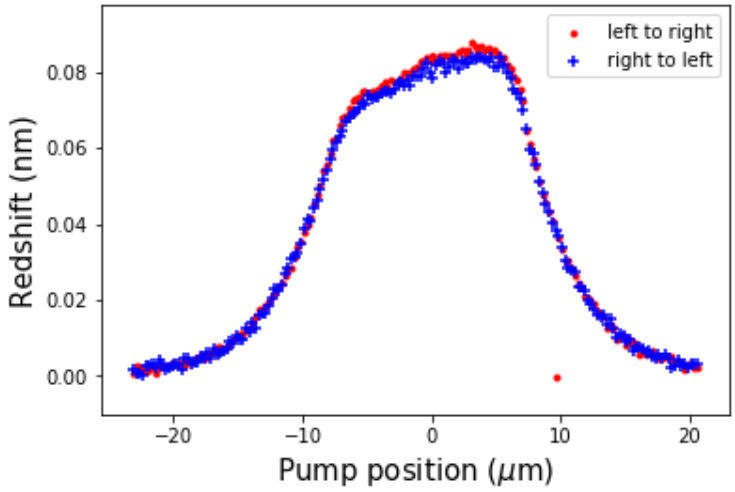

Figure 12: Redshift of cavity resonance for different pump positions. The red dots indicate the left-to-right scan, the blue dots the right-to-left scan. They show good agreement however this time the backwards scan is systemically less redshifted, but both scans show the same redshift profile. The red dot with zero redshift at $x = 10\ \mu\mathrm{m}$ can most likely be attributed to the shutter not opening.

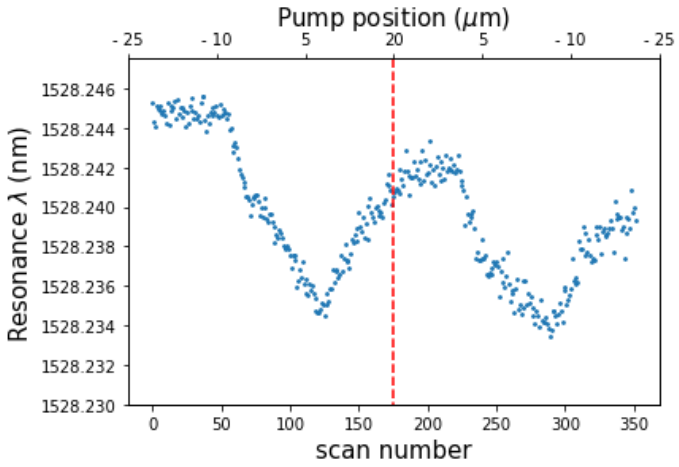

Figure 13: Plot of all the reference resonance wavelength in sequence. These values are for the entire measurement, so the back-and-forth movement of the pump beam, meaning that at the vertical line the movement of the beam reverses.

Figure 13 shows similar behaviour for the reference resonances as figure 9. The most obvious way they differ is that the blueshifting of the resonance happens earlier for this resonance and it carries on longer as well. This means that for a longer range of positions the recent illumination of the sample by the blue laser beam still has effect. This provides further evidence for the delocalisation of the mode profile along the waveguide direction.

For this resonance we also observe an increase of the FWHM of the OOPS spectrum, how-

ever this time the increase is much smaller relatively. It is more difficult to discern a profile however it seems to roughly follow the redshift profile.

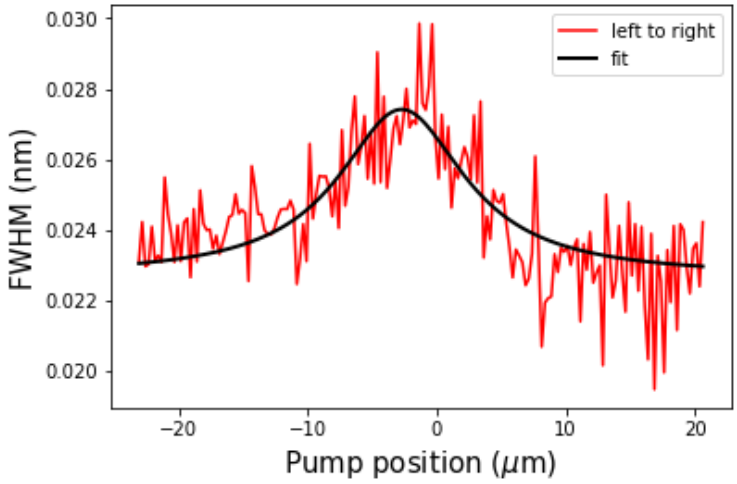

Figure 14: FWHM as a function of pump position. The right-to-left scan has been omitted for the reason that OOPS signal decreased during the measurement, possibly due to the fiber drifting away, which made the signal too noisy to accurately determine the FWHM. The FWHM of the Lorentzian fit is 12 ± 1.2 µm which is significantly narrower than the redshift profile in figure 12.

5.5 Two-dimensional scan

To uncover any two dimensional information about the mode profile of a resonance, a two dimensional pump scan is performed. Here we show the results of such a two dimensional scan; however due to the low spatial resolution that has been used little new information is uncovered. Still, these measurements do function as a proof-of-concept and show some information about the mode profile.

Figure 15 shows the two-dimensional redshift profile for the same resonance as in section 5.4.1 with λ =1530.8 nm. For this measurement a region of 26 µm x 21 µm was divided up in a 30x30 grid. This grid was scanned with the pump beam in a zigzag pattern, starting from the top row scanning left-to-right and the next row from right-to-left etc. This was done to avoid having to make large steps with the FSM while also avoiding scanning certain positions twice to save time, since this measurement already took quite a long time (almost 3 hours). This is also the reason why the spatial resolution is fairly low, especially when compared to the one-dimensional scans.

The shape of the redshift profile is not quite circular, indicating that the electric field profile is much more stretched in the x directing than in the y direction. Using these measurements it is not possible to discern any of the finer details of the mode profile; for this goal a higher spatial resolution combined with a deconvolution of the redshift profile need to be used.

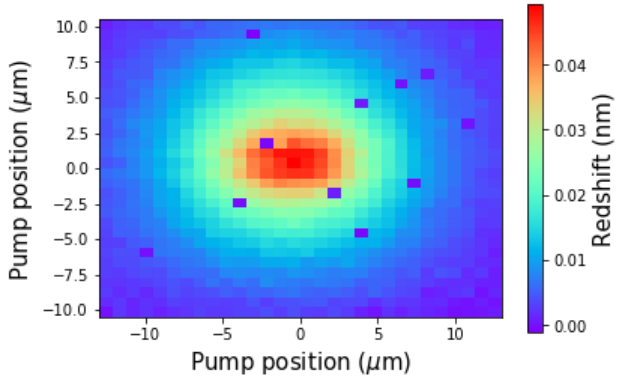

Figure 15: Redshift of resonance as a function of pump position. The unexpected zero redshift areas are due to the shutter malfunction. $y = 0$ corresponds to the vertical position of the cavities.

5.6 Conclusion

Our results have shown multiple effects of the local heating on resonances. We observe the redshift of resonance wavelengths which depends on the location that is heated by the pump beam. The redshift profile is not identical for different resonances: this reveals that the electric field profiles for different resonances are quite different. Furthermore, we observe that the width of the resonance in OOPS spectra is strongly dependent on the local heating. Interestingly, the redshift and change in FWHM are not perfectly correlated. Finally, we observe the blueshifting of the resonance after the sample has been illuminated with the blue laser light. The cause of this effect is unclear, but it might be due to the evaporation of a thin water film on the sample or slight ionisation of the sample.

5.7 Outlook

Using our methods of measuring redshift profiles, one could calculate the electrical field mode profile using a deconvolution of the redshift profile using the thermal profile. The level of detail that is able to be resolved is limited by the width of the thermal profile and by the spatial resolution of the scanning with the pump beam. The width could be decreased by changing the surrounding material of the membrane with a material with higher thermal conductivity, i.e. helium or water, or using a laser with a shorter wavelength to be able to more narrowly focus the pump beam. A downside is that a shorter wavelength is more damaging to the sample.

To study the origin of the blueshifting of the resonance wavelengths, one could use a different wavelength laser for the pump spot. A longer wavelength should lead to less blueshift, a shorter wavelength should lead to more blueshift, if the blueshift is caused by the ionising radiation. It might also be possible to *use* the blueshifting to uncover to mode profile: the blueshift is also caused by a slight pertubation of the local dielectric constant. For the thermal redshift, this perturbation is tied to the width of the thermal profile. However, for this blueshift it might be tied to the width of the beam spot, which is much narrower than the

thermal profile. Since the beam spot is narrower than the thermal profile, finer details of the mode profile can be probed. Actual measurements using this method might be cumbersome due to the long time scale of the effect as can be seen in figures 9 and 13, which show the long duration of the build-up and decay of the blueshift.

Further research is required for understanding the increase in FWHM as a function of pump position. This might reveal information about the origin of the Q-factor of resonances. Using a higher pump power, the FWHM profile should be more easily discernible.

6 References

[1] N. W. Ashcroft and N. D. Mermin, *Solid state physics*, ch. 1. Cengage Learning, 1976.

[2] J. D. Joannopoulos, P. R. Villeneuve, and S. Fan, "Photonic crystals: putting a new twist on light," *Nature*, vol. 386, no. 6621, p. 143, 1997.

[3] Y. Akahane, T. Asano, B.-S. Song, and S. Noda, "High-q photonic nanocavity in a two-dimensional photonic crystal," *Nature*, vol. 425, no. 6961, p. 944, 2003.

[4] S. Sokolov, J. Lian, E. Yüce, S. Combrié, G. Lehoucq, A. De Rossi, and A. P. Mosk, "Local thermal resonance control of gainp photonic crystal membrane cavities using ambient gas cooling," *Applied physics letters*, vol. 106, no. 17, p. 171113, 2015.

[5] S. Sokolov, *Dynamic tuning of photonic crystal nanocavities*. PhD thesis, Universiteit Twente, 2017.

[6] E. Logothetis and P. Hartman, "Laser-induced electron emission from solids: many-photon photoelectric effects and thermionic emission," *Physical Review*, vol. 187, no. 2, p. 460, 1969.

[7] J. D. Joannopoulos, S. G. Johnson, J. N. Winn, and R. D. Meade, *Photonic crystals: molding the flow of light*, ch. 2, pp. 17–19. Princeton university press, 2011.

[8] J. Lian, *Control of resonances in photonic crystal waveguides*. PhD thesis, Universiteit Twente, 2016.

[9] Newport Corporation, *FSM-300 User's manual*, 2014.

[10] E. Hecht, *Optics*, ch. 5, pp. 246–252. Pearson Education, 2014.

[11] J. D. Joannopoulos, S. G. Johnson, J. N. Winn, and R. D. Meade, *Photonic crystals: molding the flow of light*, ch. 10, pp. 199–203. Princeton university press, 2011.

A Image of sample

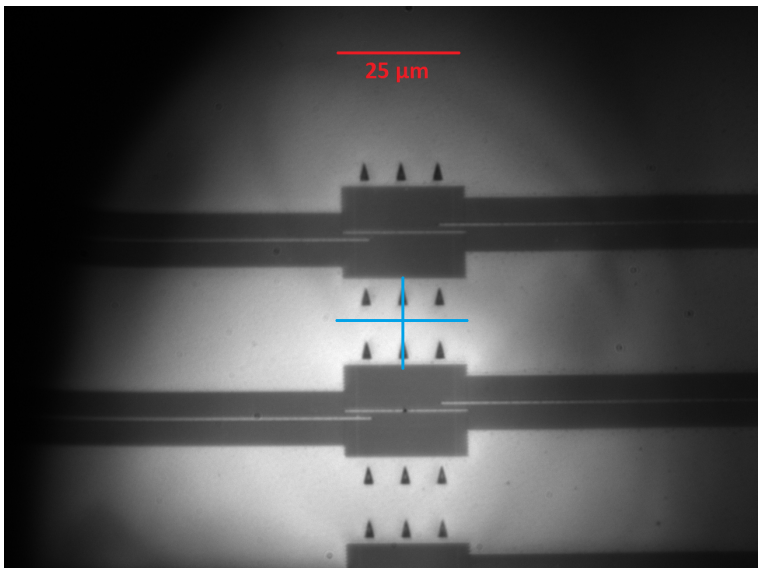

Figure 16: Image of of sample made using the blue camera. The blue cross indicate the range that was used for the calibration of the FSM.

B Calibration using entire camera

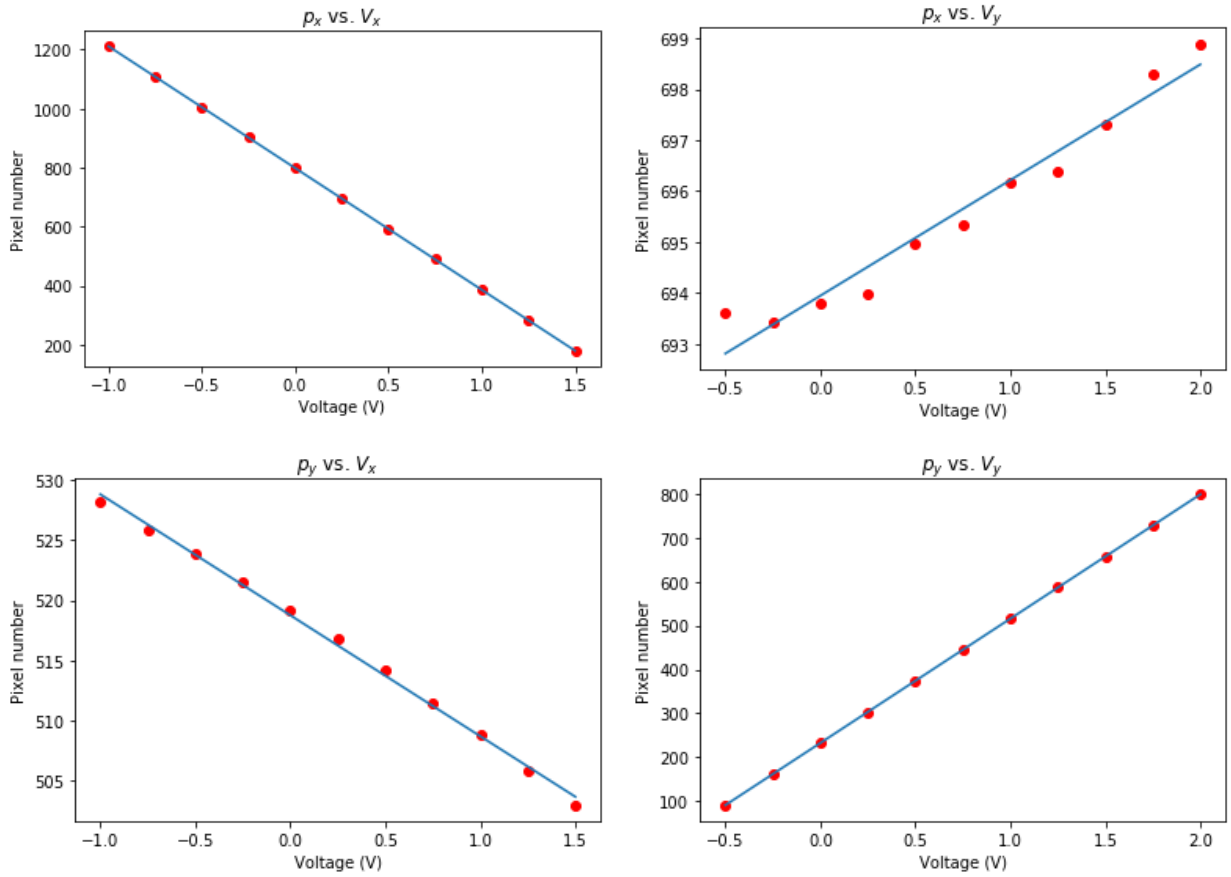

Figure 17: Fits to the beam positions when the entire camera is used for the calibration. Especially the top-right and bottom-left fits show that the response of beam position to changes in the FSM voltages is non-linear.

C Reference measurements for two resonances

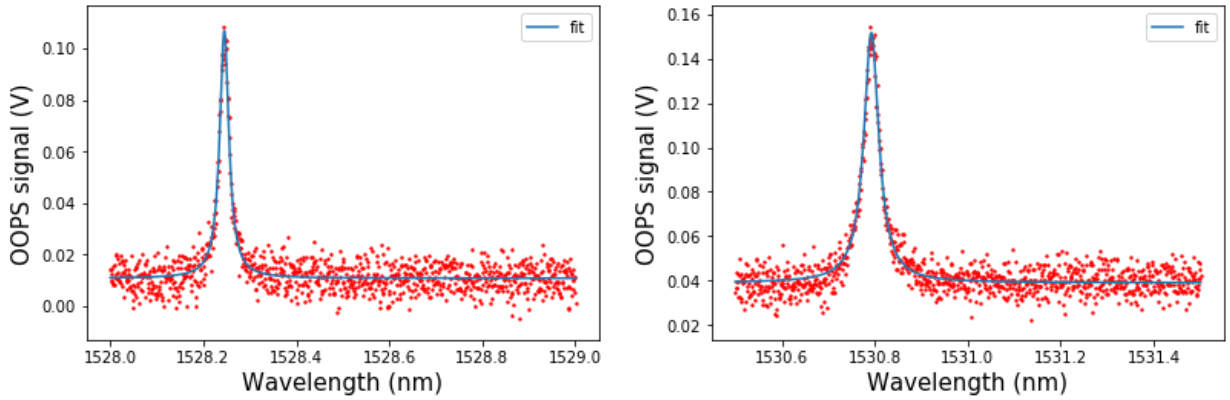

Figure 18: Examples of the unpumped cavity response for the resonances studied in section 5.

D Additional fits for FWHM measurement

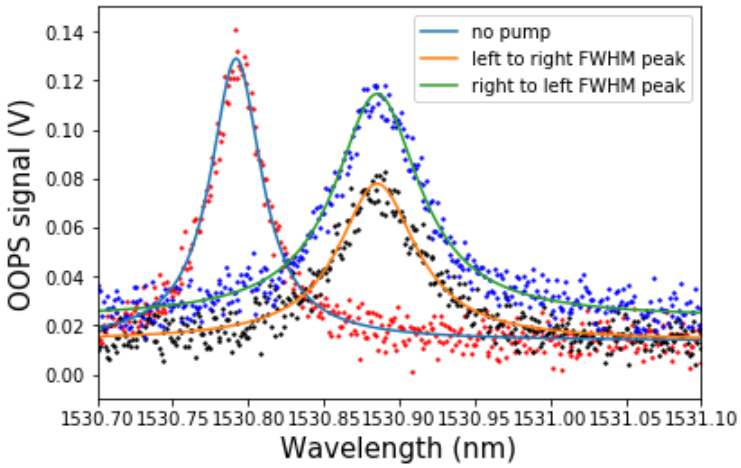

Figure 19: Additional fits showing that the FWHM increases and that the pump light does not push the resonances into a non-linear regime. The right-to-left peak is significantly higher than the left to right peak because both the noise level and strength of the signal increased during the measurement.

E Datasets and analysis scripts

Data used for results in section 5.4.1 is *Data_20181129_15h42m59s.hdf5*
Data used for results in section 5.4.2 is *Data_20181129_11h57m54s.hdf5*
Data used for results in section 5.5 is *Data_20181214_11h57m54d.hdf5*

Script used in section 4 for the calibration is *Calibration_script.py*
Script used in section 5 for the analysis of the measurements is *Linescan_analysis_script.py*